Geophys. J. Int. (2006) **166,** 33–45 doi: 10.1111/j.1365-246X.2006.02898.x

Intersections of remanence small circles: new tools to improve data processing and interpretation in palaeomagnetism

Martin Waldhör and Erwin Appel

Institute for Geosciences, University Tübingen, Sigwartstr. 10, D-72076 *Tübingen, Germany. E-mail: martin.waldhoer@uni-tuebingen.de*

Accepted 2006 January 1. Received 2005 December 14; in original form 2005 June 10

SUMMARY

Intersections of remanence small circles are increasingly used in palaeomagnetism to determine the palaeofield direction from synfolding remanences. The approach ['small circle intersection (SCI) method'] presupposes that remanence small circles from sites tilted to different directions intersect in a common point, which is assumed to represent the palaeofield direction. The SCI method is not restricted to synfolding remanences. It can be applied also to derive the palaeofield direction from pre-folding remanences, in addition to tilt correction and as a cross-check for fold tests. However, the SCI method has specific requirements and does not work in all cases. The suitability of data sets and reliability of palaeofield estimates have to be assessed carefully and always against the background of local geology. This paper examines the occurrence and distribution of SCI as a tool of judgement: first, a data set is most suitable and a palaeofield estimate by SCI most reliable, when most of the theoretically possible intersections are realized and, in addition, clearly grouping in a narrow region. Second, the small circles that greatly determine the result of SCI, are identified by the highest number of intersections they have with the others. These criteria allow a systematic investigation of SCI estimates upon stability and dependencies. Moreover, SCIs can be an indicator of irregular, unexpected tectonic settings. When the intersections disperse strongly although significant bedding strike differences are given, relative rotations or other unexpected displacements are likely to have occurred. If so, the SCI estimate will be invalid and probably biased, however, also Fisher mean calculation and most fold tests will be affected. In this case, the SCIs can help to separate the data into subsets valid for Fisher statistics and SCI methods. The other possibility is to use tentative reconstructions to infer the true sequence of tilts and rotations and correct the data adequately.

Key words: fold tests, palaeomagnetism, small circles.

1 INTRODUCTION

Palaeomagnetism focuses increasingly on secondary remanences from orogenic regions. These remanences are often synfolding, having been acquired at an intermediate stage of folding and then been tilted further. In this case, conventional tilt correction with associated fold tests can no more derive the palaeofield direction. An alternative approach, independently found by McClelland-Brown (1983), Surmont *et al.* (1990) and Shipunov (1997), is becoming used increasingly: these authors noted that remanence small circles retain the information about the palaeomagnetic field in their intersections with each other. The first two authors used stepwise differential untilting to estimate the palaeofield direction, and the latter an analytical approach with iterative determination. As all the approaches base on the same principle, that is, intersecting small circles, they will further on be referred to as 'small circle intersection (SCI) methods'. Several authors have already applied SCI methods successfully to synfolding data (Enkin *et al.* 2000; Henry *et al.* 2001; Jordanova *et al.* 2001; Lewchuk *et al.* 2002; Enkin *et al.* 2002). However, there are also publications where biased field estimates turned out (Cairanne *et al.* 2002; Delaunay *et al.* 2002) and a general applicability has been questioned. SCI will of course not work in all cases because it requires appropriate tectonic conditions, that is:

(1) The remanence small circles have to intersect. A concentric fold where all bedding strikes (usually assumed to represent the tilt axes) are more or less parallel, will unlikely provide intersecting small circles. SCI requires sites from layers with sufficiently differing bedding strikes, for example, from a heterogeneous, curved fold geometry or from disconnected tilt blocks in a larger sampling area.

(2) Between the sites no differential rotations around vertical and other axes not parallel to bedding strike must have occurred. They would displace the SCIs and bias the SCI estimate.

SCI is an important approach in palaeomagnetism, because it can be applied not only to synfolding, but as well to pre-folding data. This has not yet been recognized adequately in palaeomagnetism. SCI is in fact a further method to assess the remanence character, in

addition and as a cross-check to the common fold tests. However, many palaeofield estimates with SCI are determined by only one or a few sites, having a strongly different bedding strike with respect to the others. If tectonic rotations had affected these sites, the palaeofield estimate could be biased completely. Henry *et al.* (2004) have already used bootstrap statistics to derive uncertainty regions for SCI estimates, accounting for the influence of bedding geometry and showing uncertainties of palaeofield estimates. In this paper we introduce further concepts of how to assess the reliability of SCI estimates. They base on SCIs and allow to recognize which and how many sites play a determining role for the SCI methods. Moreover, the intersections can show whether a data set meets the common tectonic assumptions of palaeomagnetism, or whether irregularities like relative vertical-axis rotations or subsequent tilts are hidden.

2 THE BASIC IDEA OF SMALL CIRCLE INTERSECTIONS

When applying tilt correction, palaeomagnetism usually assumes that a tilted remanence has been rotated around a horizontal axis parallel to bedding strike. Fig. 1(a) illustrates the basic geometry of this tilting process: the vector normal to the bedding plane (bedding pole) moves on a great circle, called π*-circle* of bedding (e.g. Ramsay & Huber 1987). Likewise, a remanence vector tied to this layer will move along a small circle, the *remanence small circle*. Remanence small circle and corresponding π-circle are parallel and vertical for a horizontal tilt axis; their $x- -y$ distance as a fraction of the radius ($r = 1$) is a function of palaeofield inclination and tilting direction (Waldhör *et al.* 2001).

McClelland-Brown (1983), Surmont *et al.* (1990) and Shipunov (1997) recognized that the small circles of remanences tilted to different directions will intersect in a common point (in practise a narrow region), which indicates the palaeomagnetic field direction during their acquisition (Figs 1b and c). Intersections are independent from where on a small circle a remanence lies. To estimate the palaeofield direction, McClelland-Brown (1983), Surmont *et al.* (1990) and later Enkin *et al.* (2000, 2002) have used optimum differential untilting to find highest vector concentration between 0 and 100 per cent untilting for each site, but did not publish the procedures in detail. Shipunov (1997) instead presented a practical least-squares method to derive the palaeofield direction (see appendix). It determines the point in the $x- -y$-plane of the projected unit sphere that lies closest to all involved remanence small circles. Henry *et al.* (2004) pointed out that Shipunov's geometrical approach might produce a bias due to the use of $x- -y$ distances instead of angles. We, therefore, used a modified method in addition, which is documented in the appendix. A sound comparison of the different SCI methods would require extensive computer simulations, which is not the subject of the current paper, yet a further task for the future. In practise, however, Shipunov's method and our modification yielded very similar results. As a new feature, we calculated contour plots of the fit parameter to graphically illustrate properties and result of SCI estimates, and determined percentage of untilting.

An important aspect of SCI methods is that they do not distinguish between upper and lower hemisphere. Geometrical symmetry (see Fig. 1c) causes highest vector concentration to be found twice, for positive and negative inclination, for example, $D/I = 0°/+5°$ and $D/I = 0°/-5°$ are equivalent solutions and not far apart. This must be kept in mind when SCI is applied to data with shallow palaeofield inclination.

3 INTERSECTIONS NUMBERS AND RATIOS

Whether remanence small circles intersect, depends first of all on how much the bedding strikes of a data set vary. Fold belts generally have a directed regime of deformation where bedding strikes, which are not perpendicular to the shortening direction would not be expected very often. However, in practise they occur far more frequently. Fig. 2 depicts the actual variation of tilt axes from 60 palaeomagnetic studies of fold belts. Most data sets exhibit a considerable variation of their bedding strikes. A purely concentric fold geometry with parallel bedding strikes throughout is rather the exception than the rule.

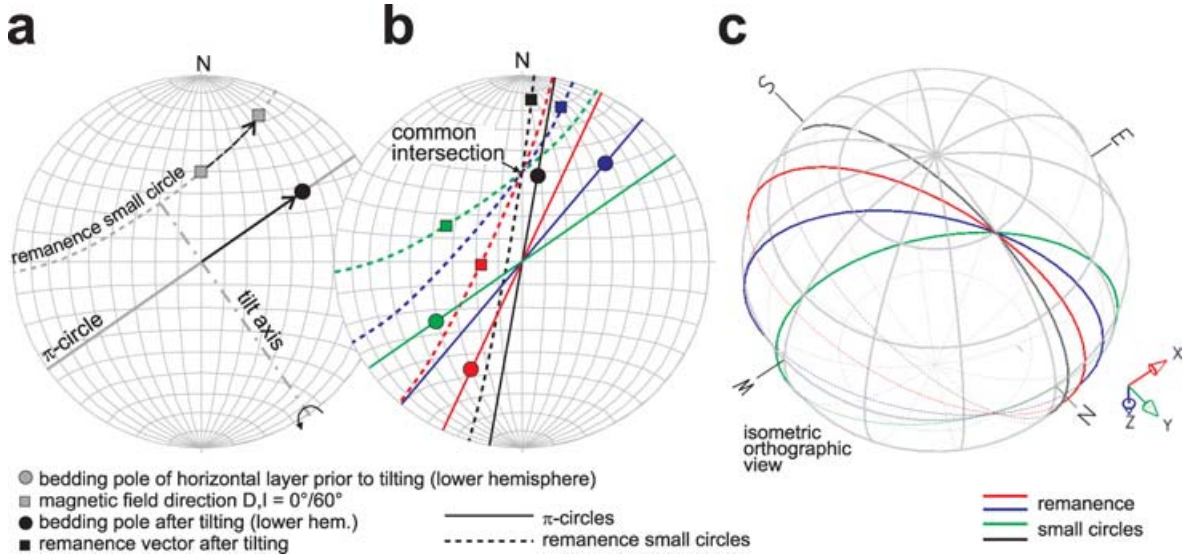

Figure 1. Basic geometry of tilting. (a) Tilting of a layer around a horizontal axis moves the bedding pole on a great circle (π-circle) and the associated remanence vector on a parallel small circle. (b) Remanence small circles for different tilting directions intersect in a common point, the palaeofield direction (Shipunov 1997). (c) Perspective view onto the small circles and their intersection (view onto the lower hemisphere; π-circles, bedding poles and remanences omitted for clarity). Note that remanence small circles intersect twice, on lower and upper hemisphere.

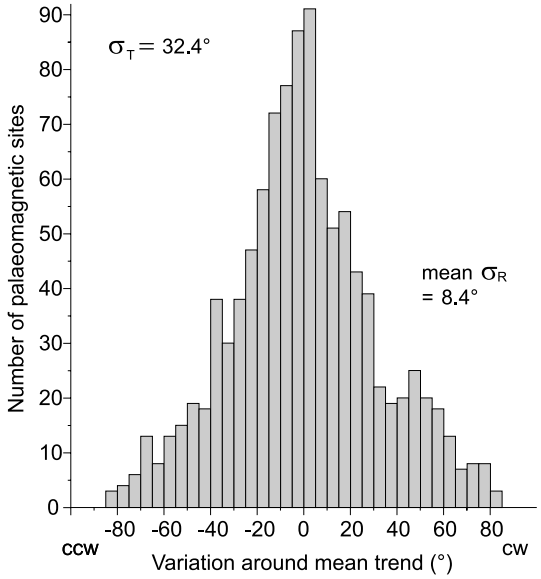

Figure 2. Variation of bedding strikes (usually = tilt axes) in palaeomagnetic studies from literature. 1056 tilt axes (each from one palaeomagnetic site) from 60 structurally contiguous data sets (references below). Variation around respective mean trend has been determined for each data set separately (using the closest grouping of trends in each case). Overall standard deviation of trends is $\sigma_T = 32.4°$. Average standard deviation of remanence inclination is $\sigma_R = 8.4°$ (pre-folding data sets only). Data from Gough & Opdike (1963), Klootwijk & Bingham (1980), Lin Jinlu & Watts (1988), Otofuji *et al.* (1989), Sharps *et al.* (1989), McFadden (1990), Channell *et al.* (1992a,b), Chen *et al.* (1992), Hirt *et al.* (1992), Huang *et al.* (1992), Klootwijk *et al.* (1994), Thomas *et al.* (1994), Cogné *et al.* (1995), Haihong *et al.* (1995), Patzelt *et al.* (1996), Mac Niocaill *et al.* (1998), Haubold *et al.* (1999), Liu & Morinaga (1999), Thomas *et al.* (1999), Uno (1999), Arriagada *et al.* (2000), Huang *et al.* (2000), Mac Niocaill (2000), Pueyo (2000), Henry *et al.* (2001), Jordanova *et al.* (2001), Waldhör *et al.* (2001), Enkin *et al.* (2000, 2002), Kravchinsky *et al.* (2002), Schätz *et al.* (2002), Zwing *et al.* (2002), Enkin (2003), Halim *et al.* (2003), Levashova *et al.* (2003), Lewchuk *et al.* (2003), Molina-Garza *et al.* (2003), Niitsuma *et al.* (2003), Henry *et al.* (2004), Pueyo *et al.* (2004), Staiger (2004), Tamai *et al.* (2004), Uno *et al.* (2004), Huang *et al.* (2005).

In order to assess the significance of intersections and the suitability of a data set for SCI, the definition of a minimum angle between small circles could be considered, for example, at least three times the α_{95}-angle of the site means or similar. In practise, however, remanence small circles can enclose a significant angle and still do not intersect, for example, due to tectonic rotations. On the other hand, they may have low angles with each other, but intersect in a narrow region which correctly reflects the field direction. To have a further tool of judgement, we examined the numbers of intersections. The basic idea involves two aspects: First, the more intersections a data set has, the better its SCI estimate is defined. Second, the more intersections an individual small circle has (the more others it crosses), the more influence it will have upon an SCI estimate.

Theoretically, a number of n remanences tilted to different directions will cause m intersection points of its small circles:

$$m = n(n-1)/2. \quad (1)$$

An individual remanence small circle can have up to $n-1$ intersections. The inherent scatter of remanences will erase intersections; erasure will be stronger when tilt axes have less variation, remanences scatter more and field inclination is shallower. We performed simulations to see in detail how the overall number of intersections depends on these factors.

In the simulation synthetic data sets have been generated iteratively, each one consisting of 20 remanences with 20 associated tilt axes. The tilt axes were drawn randomly from a Gaussian distribution (see Fig. 2) using a mean trend of 90° (N–S shortening) and standard deviations σ_T between 5° and 60° in steps of 5°. The remanence vectors were created similarly, generating D and I values for a 2-D Gaussian distribution around $D/I = 0°/0°$ using standard deviations σ_R between 2° and 20°. To produce steeper field inclinations, the remanence vectors were rotated around a horizontal axis trending 90°. Fig. 3(a) gives an example for one of these data sets, showing tilt axes distribution, remanences and associated small circles for a magnetic field of $D/I = 0°/55°$. Fig. 3(b) charts the ratio of realized to possible intersections depending on field inclination for $\sigma_T = 10°$, 30° and 50°. Every data point represents the average from 200 independently created data sets with tilt axes and remanences.

For the average variation of tilt axes as shown in Fig. 2 ($\sigma_T \approx 30°$), the intersection ratio m_r/m_P ranges between 0.46 and 0.49 for $I = 0°$ (Fig. 3b). With a higher variation of tilt axes the ratio moves slightly above 0.5 at $I = 0°$. With lower σ_T-values the curves differ stronger, showing that the intersection ratio becomes more sensitive to remanence scatter. Towards steeper field inclinations, the ratios rise generally. The rise is stronger with a better grouping of the remanences and a higher variation of the tilt axes (lower σ_R and higher σ_T). Fig. 3(c) plots the intersection ratio m_R/m_P against the ratio σ_T/σ_R for three different field inclinations and three different σ_R-values. It becomes evident that at a given field inclination, the intersection ratio depends primarily on the ratio of tilt axis variation to remanence scatter, and only to a minor extent on the absolute values of σ_T and σ_R. Fig. 3(d) shows the curves for $\sigma_R = 8°$, which represents approximately the average scatter of remanences (see Fig. 2). It is seen that the curves have a strong rise until a σ_T/σ_R-ratio of about 1.5 to 3, where the variation of the tilt axes clearly exceeds the dispersion of the remanences. Above a ratio of $\sigma_T/\sigma_R = 3$, the further increase is more or less gradual. Most practical data sets range within $\sigma_T/\sigma_R = 2$ and 6; ratios above 10 are usually not realized.

The ratio σ_T/σ_R indicates how many intersections can be expected in specific data set, however, it can eventually not tell if a SCI estimate is reliable or biased. This has to be inferred individually for each data set, taking into account the local tectonic setting and expected remanence direction. Nevertheless, the simulations together with practical experience from about 60 data sets suggest two preliminary conclusions:

(1) Below a ratio of $\sigma_T/\sigma_R = 1.5$ (dispersion of tilt axes 1.5 times higher than dispersion of remanences) data sets will unlikely provide a well constrained and reliable SCI estimate.

(2) With less than half of the possible intersections a SCI estimate is usually not reliable.

4 EXAMPLES

The following examples examine real data sets upon intersection numbers and reliability of SCI estimate. In Fig. 4(a) the remanence small circles have subparallel orientation due to similar bedding strikes. With a ratio $\sigma_T/\sigma_R = 0.43$, variation of tilt axes is below remanence dispersion. Ten sites would allow 45 intersections, 16 of which are realized in the projection circle, giving an intersection ratio of 0.36. The individual small circles do not have more than

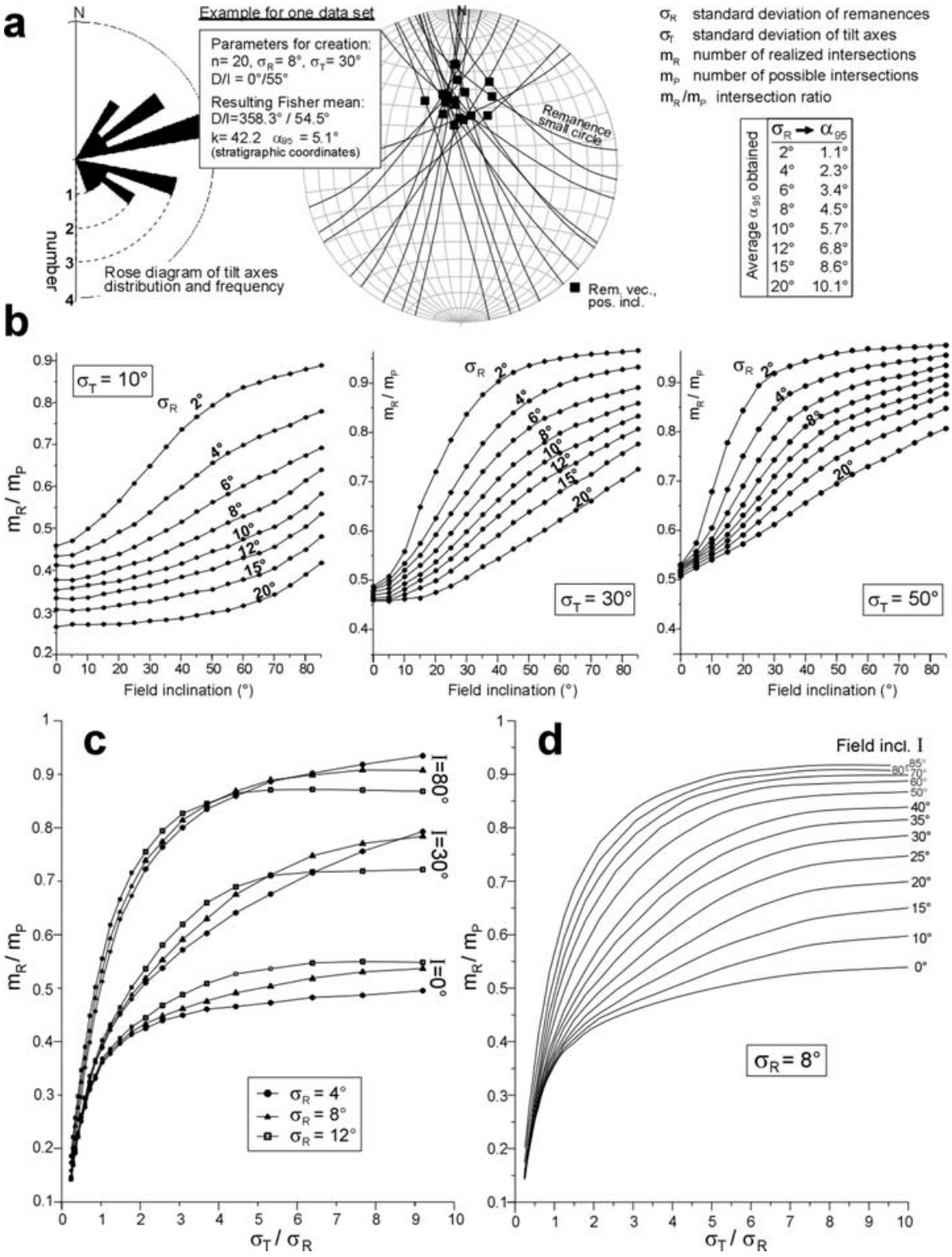

Figure 3. Simulation of intersection ratios depending on variation of tilt axes (σ_T), remanence scatter (σ_R) and field inclination using synthetic data sets. Range of σ_T: 5°–60° in steps of 5°; range of σ_R: 2°, 4°, 6°, 8°, 10°, 12°, 15° and 20°; range of field inclination: 0°–85° in steps of 5°. (a) One of about 180.000 synthetic data sets (remanence vectors with associated tilt axes) with n = 20 sites, drawn randomly from a Gaussian distribution with standard deviation of $\sigma_T = 30°$ for the tilt axes and $\sigma_R = 8°$ for the remanence declination and inclination at 0° of inclination. Inclination of 55° obtained by subsequent tilt of vectors around horizontal E–W trending axis. Small table gives obtained α_{95}-angles for σ_R-values. (b) Plots showing ratio of realized (m_R) to possible number (m_P) of intersections, depending on field inclination, remanence scatter (σ_R) and tilt axes variation for $\sigma_T = 10°$, 30° and 50°. Each data point represents the average from 200 randomly created data sets. (c–d) Intersection ratio m_r/m_P as a function of the ratio σ_T/σ_R. In (c) curves for three different σ_R-values (remanence scatter), for three field inclinations; different absolute values for σ_T and σ_R cause only minor variation compared to the influence of field inclination. In (d) curves for $\sigma_R = 8°$ (corresponding to average remanence scatter) for field inclinations between 0°–85°. See text for discussion.

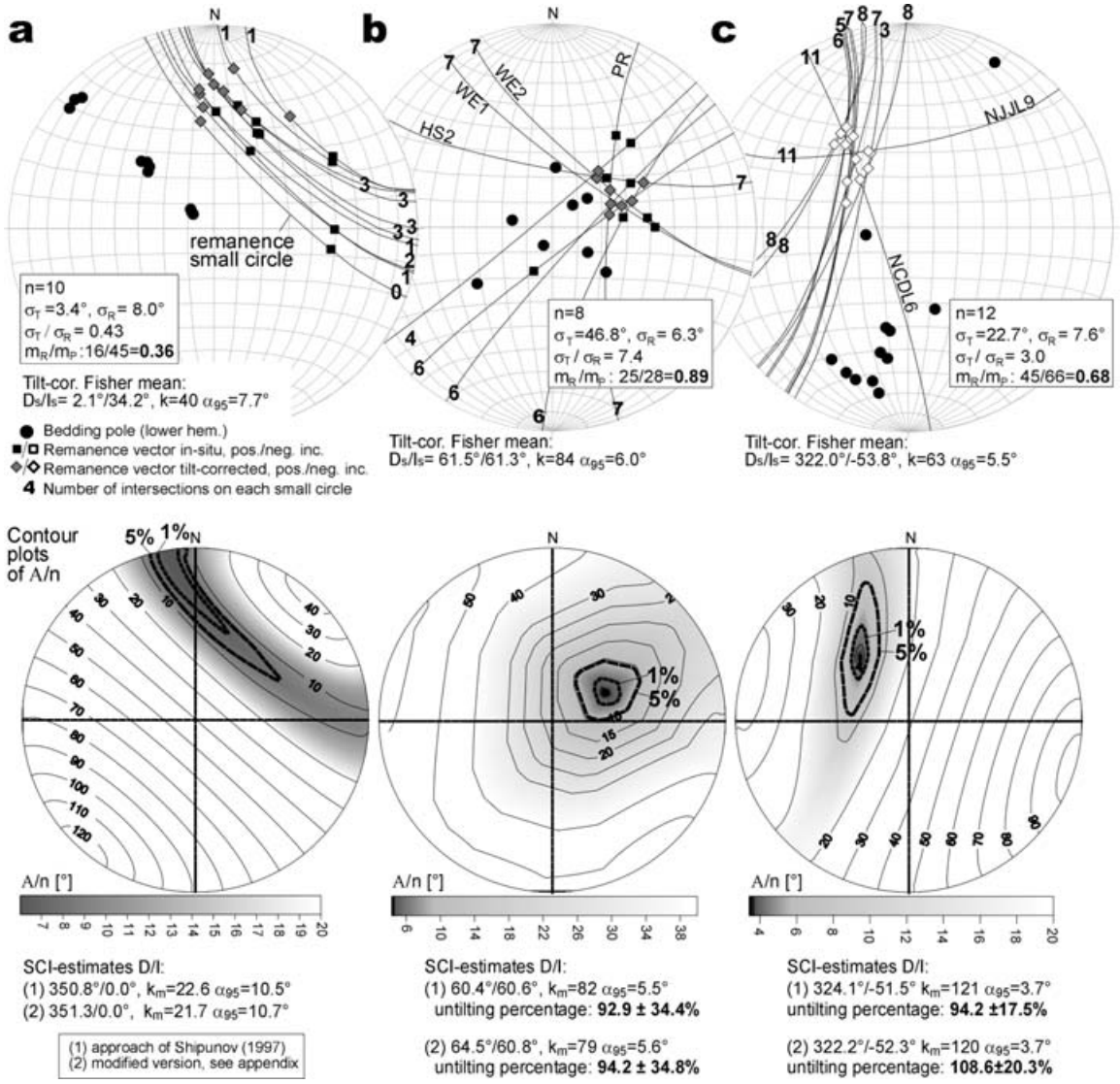

Figure 4. SCI applied to exemplary data sets from literature, both approach of Shipunov (1997) and modified version (see appendix). Upper row: data sets with remanences, bedding poles, small circles, and intersection ratios and numbers. Site labels, where given, from original publications. σ_T: standard deviation of tilt axes. σ_R: standard deviation of tilt-corrected inclinations and declinations, determined after transforming the whole (previously tilt-corrected) vector array to the equator where the overall Fisher mean achieves $I = 0°$, via rotation around a horizontal axis with trend $D_S \pm 90°$ (D_S: tilt corrected declination). m_R/m_P: intersection ratio: realized/possible number of intersections. Lower row: contour plots in equal-area projection of A/n (fit parameter of SCI; method of appendix) for a circular $x- -y$-grid with nodes every 0.01. 1 per cent and 5 per cent contours delineate areas where the 1 percentile and 5 percentiles of the lowermost A/n-values plot. k_m: modified k-value after Enkin *et al.* (2002). Untilting percentage is average of angles necessary to rotate *in situ* remanences along their small circles to respective positions closest to SCI estimate, divided by average angle of bedding dip; error interval is standard deviation. (a) Data set (McFadden 1990, Table 5 therein) with subparallel small circles having low intersection numbers. Lower 1 percentile and 5 percentile areas of A/n-values are strongly elongated and open up towards the border of the unit circle. (b) Data set (Channel *et al.* 1992a, *Wolfgangsee*) with high intersection numbers and a well-constrained SCI estimate. (c) Data set (Klootwijk *et al.* 1980, *Thakkhola*) where two deviating small circles dominate the SCI estimate. See text for further discussion.

three from nine possible intersections. When SCI (both method of Shipunov and our modification) is applied iteratively, the directional estimates shift to the border of the sphere to about $D/I = 351°/0°$. As such a direction is far off the *in situ* and tilt-corrected remanence directions, SCI is most likely biased completely and invalid.

In Fig. 4(b), the small circles reflect four to five significantly different bedding strikes. Tilt axis variation is much higher than remanence dispersion. With an intersection ratio of 0.89, most intersections are realized. Four sites have the maximum of seven intersections, three sites have six intersections and only one has four. The SCI estimate is, therefore, supported broadly by most of the sites. The contour plot shows accordingly a clearly defined minimum of A/n within the unit circle. The corresponding field direction agrees well with the tilt-corrected overall mean and provides an untilting percentage around 100 per cent, confirming a pre-folding remanence character.

In the data set of Fig. 4(c) only two sites have a different bedding strike. Tilt axis variation is three times higher than remanence dispersion. 45 of 66 possible intersections are found, corresponding to an intersection ratio of 0.68. The two deviating sites have the maximum of 11 intersections and will, therefore, govern the SCI estimate. A/n still has a clear minimum within the unit circle,

yet with elongated percentile-areas. Also here, SCI gives a direction very close to the tilt-corrected mean and untilting percentages close to 100 per cent, again confirming a pre-folding remanence character.

The examples of Fig. 4 are showing the expected behaviour. The higher the ratio σ_T/σ_R, the more intersections occur and the better constrained the SCI estimate is. Likewise, remanence small circles that greatly determine the estimate, carry the highest number of intersections. In about 60 published data sets (citations in caption of Fig. 2) we found mostly the same behaviour. In most of them, the tilting directions show considerable variations and the SCI estimates provide reasonable palaeofield directions. However, like with the fold tests, there are also cases where an SCI estimate seems well defined but in reality is erroneous. We do not think that the definition of rigid criteria like absolute and relative intersection numbers, confidence limits or significance ratios is appropriate. Instead, an individual look should be taken to the local fold geometry and tectonics, and the directional properties of each data set, particularly in the case of synfolding remanences where tilt correction is not available for comparison with SCI estimated. Especially the following issues should be addressed:

(1) Which and how many sites determine the SCI estimate?
(2) Are deviating bedding strikes the result of relative vertical-axis rotations?
(3) Are there hidden tectonic displacements such as relative vertical-axis rotations or overall tilts?

5 WHICH SITES DETERMINE THE SCI ESTIMATE?

In the fold tests it is good practise to investigate if the result depends strongly on single sites. This is done tentatively by removing one or several sites that seem important to the test. The same procedure is possible with SCI and will show which sites (remanence small circles) govern the directional estimate. Here, however, the intersection numbers of the individual small circles provide a clear criterion which sites to remove. Table 1 shows the change in the SCI estimates for the examples of Figs 4(b) and (c) when small circles with high intersection numbers are removed.

In the data set of *Wolfgangsee*, the SCI estimate is well supported by four important remanence small circles (Fig. 4b). Two of them can be removed in different selections without changing the result. Leaving out the three most important still gives a direction not too far off. Only the removal of all four small circles with seven intersections makes the SCI direction drift off completely. Thus, the field estimate is rooted broadly and can be considered as reliable. In the data set of *Thakkola* (Fig. 4c), in contrast, only one of each two important small circles can be removed without changing the SCI direction. Leaving out both makes the direction drift off strongly. Consequently, with only two from eleven sites, the SCI estimate is not broadly supported and less reliable as in the previous example.

6 DEVIATING BEDDING STRIKES: DUE TO VERTICAL-AXIS ROTATION?

Layers with bedding strikes not perpendicular to the overall shortening direction might possibly also be the product of relative vertical-axis rotation, having changed the bedding strike of a site from previously parallel alignment to present deviation. Such relative rotations, when large enough, will of course become evident from the remanence directions, but, when smaller, may easily be overlooked. Hypothetical, tentative reconstructions involving remanence directions *and* bedding poles can help to assess the likelihood of such rotations. In the data sets of Figs 4(b) and (c), there are at a first glance no such rotations evident, but this can be ensured in more detail. In Fig. 5, the sites with most deviating small circles (seven intersections) have been progressively 'restored' by vertical-axis rotations towards parallel alignment of bedding strike with the others.

In both cases, the hypothetical reconstructions rotate the respective remanences away from the others, indicated by decreasing k-values. It is, therefore, unlikely that the deviating bedding strikes are due to relative vertical-axis rotations; they most probably originated initially with folding. However, there are also cases where the contrary could be true. The data of Fig. 6 are reported pre-folding according to fold tests (Enkin 2003). Only site 77 deviates significantly with its bedding strike and, having six of seven possible intersections, determines the SCI estimate greatly. The SCI palaeofield direction, however, does not coincide with the tilt-corrected mean. The reason could be that either the data are not pre-folding, or, excluding pure remanence scatter, that a vertical-axis rotation displaced site 77 relative to the others. Effectively, rotating site 77 tentatively towards parallel bedding strike with the others shifts the associated remanence closer to the other remanences. Vertical-axis rotation can, therefore, be considered, causing an erroneous SCI estimate in this case (specific tectonic details are not given in the original publication).

Table 1. SCI estimates after selective removal of sites from the two data sets of Figs 4(b) and (c). For *Wolfgangsee* (Channell et al. 1992a), the estimate is broadly supported. For *Thakkhola* (Klootwijk & Bingham 1980) the estimate is maintained by only two important small circles. SCI estimate according to method of appendix. Method of Shipunov (1997) (not shown) yields very similar results.

	SCI estimate				
Wolfgangsee (see Fig. 2b)	D (°)	I (°)	k_m	α_{95}(°)	Untilting percentage
all sites	**64.9**	**61.5**	**79**	**5.6**	**94.2 ± 34.8 per cent**
WE1 & WE2 removed (7 intersections)	64.3	60.7	57	7.6	96.4 ± 30.5 per cent
HS2 & PR removed (7 intersections)	69.7	59.1	68	6.0	77.9 ± 46.5 per cent
WE1, WE2 & HS2 removed	69.2	66.0	60	7.4	109.8 ± 25.8 per cent
WE1, WE2, HS2 & PR removed	55.3	35.8	44	10.5	107.0 ± 177 per cent
Thakkhola (see Fig. 2c)					
all sites	**322.2**	**52.3**	**120**	**3.7**	**108.6 ± 20.3 per cent**
NJJL9 removed (11 intersections)	323.4	51.2	110	4.0	99.1 ± 17.4 per cent
NCDL6 removed (11 intersections)	322.0	52.3	108	4.1	98.4 ± 17.1 per cent
NJJL9 & NCDL6 removed	338.5	31.1	84	4.8	61.7 ± 30.5 per cent

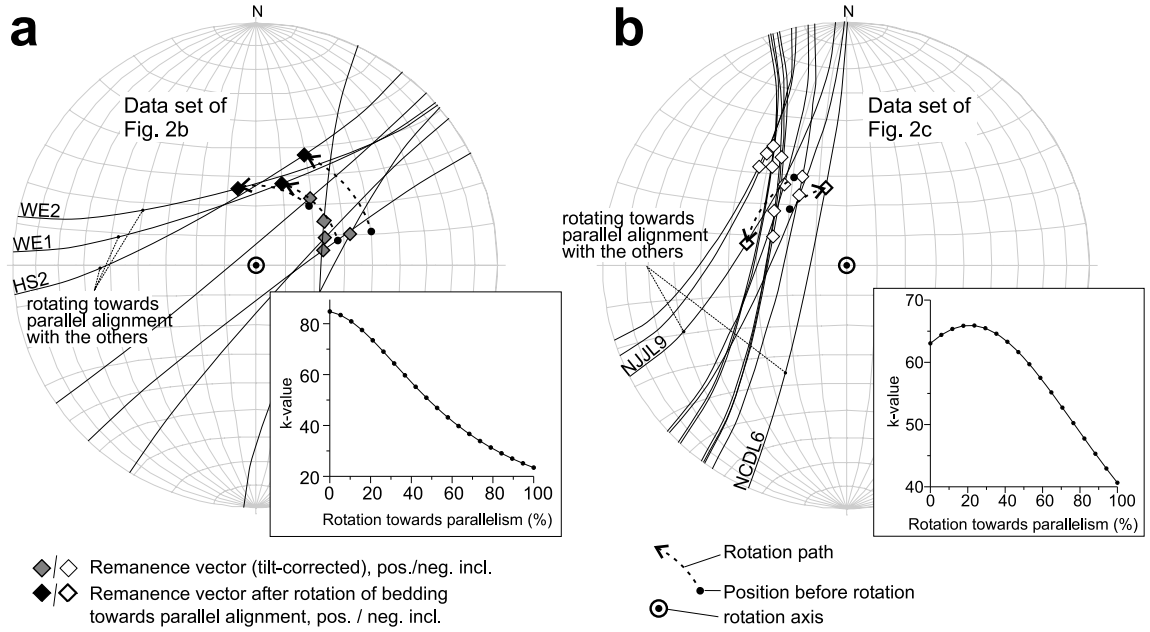

Figure 5. Hypothetical, tentative reconstructions to assess whether relative vertical-axis rotations could have caused deviating bedding strikes. Original data sets in Figs 4(b) (*Wolfgangsee*) and (c) (*Thakkola*). (a) and (b): 'Restoring' strongly deviating remanence small circles (with labels, see Fig. 4 for comparison) by proportional vertical-axis rotation towards parallel alignment of bedding strike with the others causes the associated remanence vectors to leave the grouping, progressively lowering the *k*-value of the Fisher mean. Vertical-axis rotations causing the deviating bedding strikes are, therefore, unlikely.

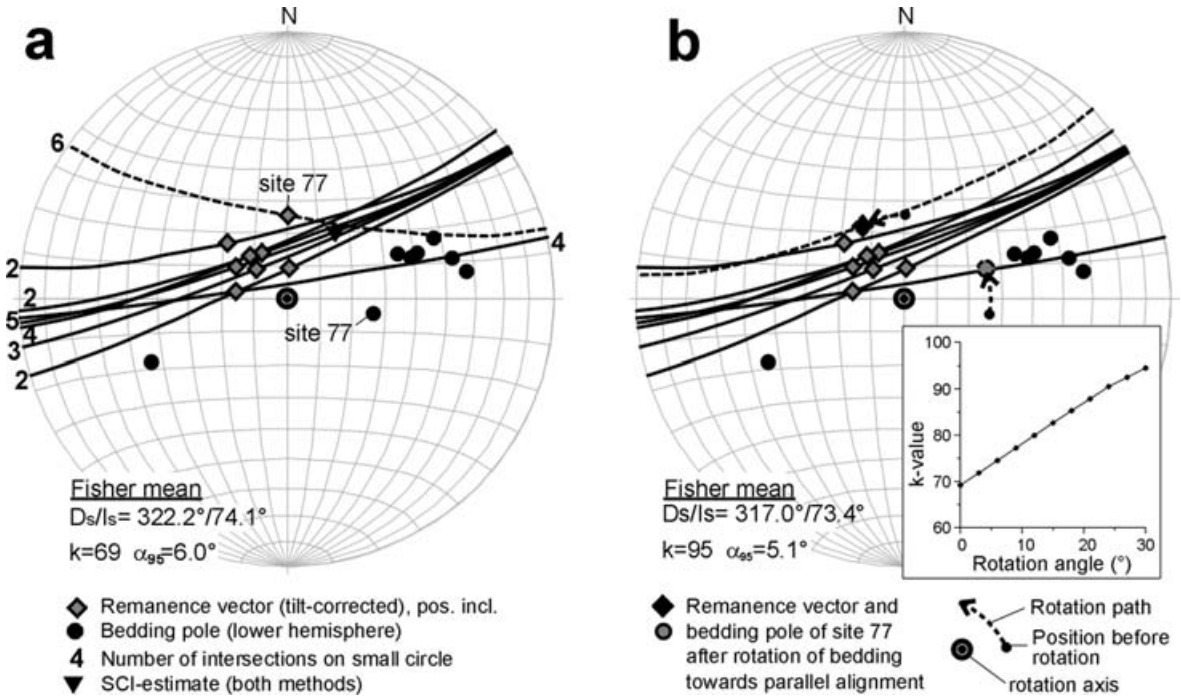

Figure 6. Data set (*Crowsnest*; Enkin *et al.* 2002; Enkin 2003) where deviating bedding strike of a site is possibly due to vertical-axis rotation. (a) Actual data set with tilt-corrected remanences and bedding poles. SCI estimate is determined strongly by site 77 and does not coincide with the tilt-corrected remanence direction. (b) Hypothetical, tentative reconstruction by rotation of site 77 towards parallel bedding strike. Concentration of remanence vectors increases all the way. Site 77 has probably been vertical-axis rotated with respect to the others, causing an erroneous SCI estimate. Equal-area projections.

7 DID HIDDEN DISPLACEMENTS BIAS SCI ESTIMATE AND TILT CORRECTION?

Several types of—from the palaeomagnetic point of view—irregular' tectonic displacements can affect the palaeomagnetic data sets: vertical-axis rotations between sites (probably the most common irregularity), a subsequent overall tilt (e.g. in plunging folds) or a second phase of folding at an angle to the first. The latter should become evident from bedding geometry in the field (see Ramsay & Huber 1987), whereas relative vertical-axis rotations and a subsequent overall tilt are certainly more difficult to identify from

structural data. When such irregular tectonic settings exist, the prerequisite assumptions of palaeomagnetic interpretation (tilt of each site around one horizontal axis, no vertical-axis rotations between the sites, no subsequent tilts oblique to the first) are no more accomplished, and conventional tilt correction with Fisher mean calculation is not appropriate. It will always be a difficult task to unravel the true sequence of tilts and rotations. Stewart (1995) and Pueyo *et al.* (2003) have addressed this problem by choosing different paths for untilting and comparing the distributions of the corrected remanences. Small circles with their intersections can provide another, additional tool to recognize unexpected tectonic settings and unravel the true sequence of deformation.

7.1 Evidence for relative rotations and other irregular displacements between sites

Fig. 6 has already given an example for an erroneous SCI result, caused by relative vertical-axis rotation of a site. Such rotations should generally be evident from the distribution of the tilt-corrected remanence vectors (declination scatters more than inclination). However, the remanences must be pre-folding to become tilt-corrected and the rotations must be large enough to clearly exceed remanence scatter. SCIs instead do not require a pre-folding remanence character and they are quite sensitive to relative displacements.

First of all, the intersections can show the absence of tectonic irregularities: when a palaeomagnetic data set has widely differing bedding strikes and the SCIs concentrate in a narrow region, where also the tilt-corrected remanences situate (coinciding palaeofields from SCI and tilt correction; for example, Figs 4b and c), we have all the available evidence for a pre-folding remanence character and a regular tectonic setting. Such a clear concentration of intersections is indeed observed in the majority of the pre-folding data sets we examined. On the other hand, there are also data sets where the intersections disperse broadly although large bedding strike differences are given. When pure remanence scatter alone does unlikely account

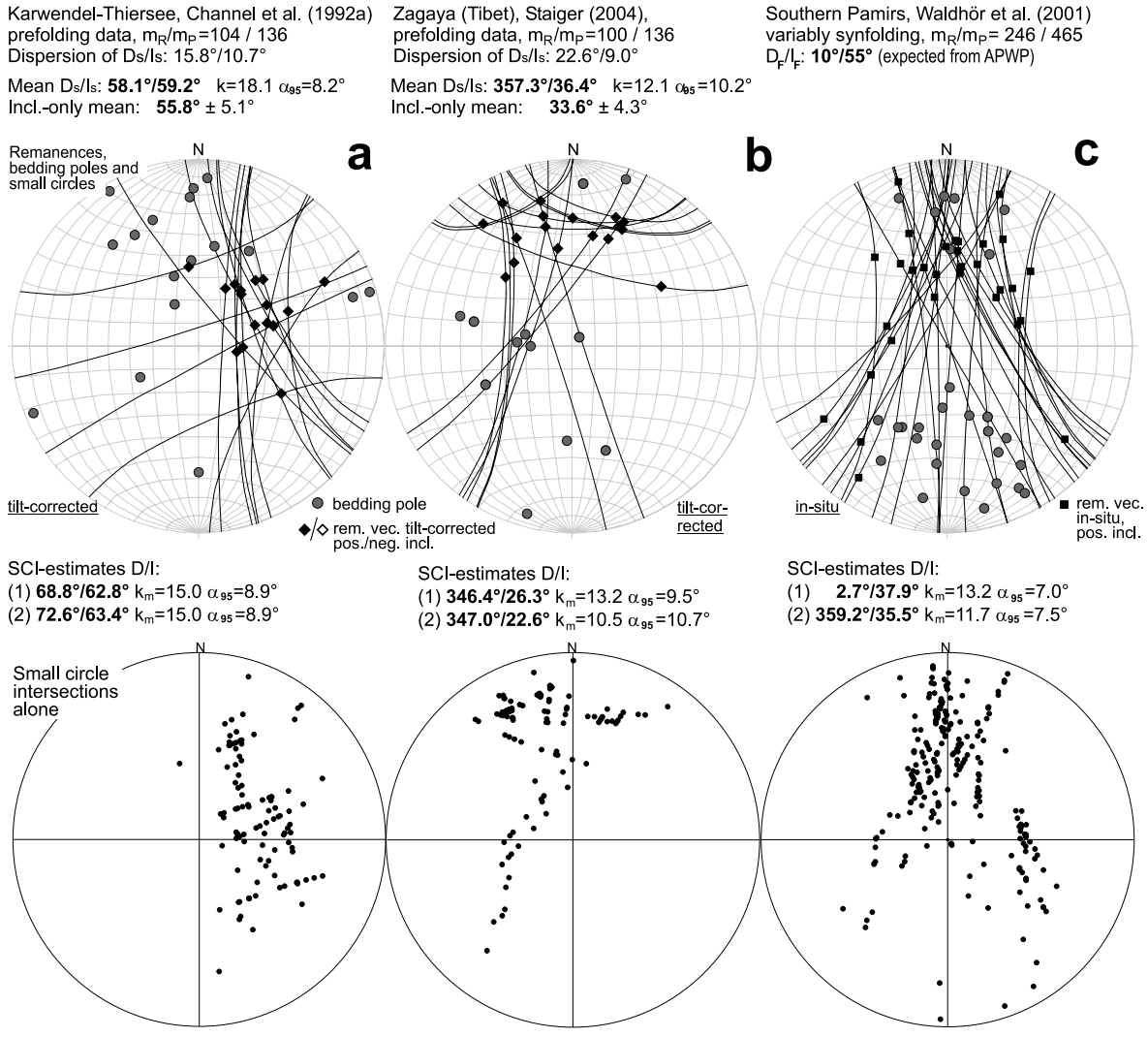

Figure 7. Data sets with a strong dispersion of SCIs, despite large bedding strike differences. (a) and (b) are pre-folding data sets, where D_S disperses stronger than I_S, probably due to relative vertical-axis rotations. (c) Synfolding data set. D_F/I_F is expected palaeofield direction from APWP (see Waldhör *et al.* 2001). In all data sets the SCI estimates (1: Shipunov's method, 2: modified method) differ significantly from the tilt-corrected Fisher mean or the expected direction. The data sets do not have appropriate geometry for Fisher mean calculation and fold tests. Equal-area projections. m_r: realized number of intersections, m_p: possible number of intersections. Dispersion D_S/I_S: see caption of Fig. 4 for determination. Mean D_S/I_S: Fisher mean of tilt-corrected remanences as published by respective authors. k_m: modified concentration parameter according to Enkin *et al.* (2002). Inclination-only means after Enkin & Watson (1996).

for, irregular tectonic displacements must come into consideration as a possible reason.

Fig. 7 depicts three data sets where the SCIs are dispersed broadly although bedding strikes show large variations. Figs 7(a) and (b) have pre-folding remanences. These two data sets give threefold evidence for tectonic irregularities: higher scatter of D_S than of I_S, non-coincidence of palaeofields from SCI estimate and tilt correction, and dispersed SCIs. In Fig. 7(c), due to the synfolding remanence character, only the SCIs can indicate the irregular tectonic setting. Such broad dispersions of intersections, warped into several directions as shown in Figs 7(a) and (b), are a characteristic feature of data sets affected by relative rotations.

As a consequence, the data sets of Fig. 7 do not meet the geometric/tectonic presumptions of palaeomagnetism. Fisher statistics and fold tests are not valid for them. The Fisher means in Figs 7(a) and (b), for instance, have inclinations biased by about 3° compared to the inclination-only means (details in Fig. 7). The data sets require a more detailed analysis accounting for the geological structure or the deformation sequence.

7.2 Testing upon overall tilts

A subsequent overall tilt, for example, in the formation of a plunging fold, changes the absolute orientation of the bedding and remanence vectors, but does not cause relative displacements between the vectors. However, by adding a second tilt not parallel to the previous tilt, the initially vertical pairs of π-circle and remanence small circle become inclined. Subsequent overall tilts are not easily identified in the field and their possible occurrence is, therefore, mostly not considered in palaeomagnetic surveys. However, when given and not accounted for, the remanence small circles are assumed to be vertical and thus assigned erroneously. As a consequence, the SCI estimate and also the result of tilt correction become biased. Fig. 8 illustrates the effect of overall tilts with the subsequent erroneous assignment of remanence small circles. It is seen that the relative positions of the small circles and their intersections change.

In both cases (tilt to W and tilt to N), the SCIs move away from their initial position and their dispersion increases. The tilt to W (Fig. 8b) shifts the intersections predominantly towards lower inclinations. The tilt to N (Fig. 8c) moves them both to lower and higher inclinations. Magnitude and direction of movements vary depending on initial bedding orientations (azimuth and dip) and the angle and direction of the overall tilt. However, there are two common features:

(1) Previously well-grouping intersections are becoming dispersed with increasing angles of overall tilt.

(2) In the case of pre-folding data, SCI estimate and tilt-corrected Fisher mean drift apart.

With these rules in mind, practical data sets can be checked upon possibly hidden overall tilts (plunging fold structures) by tentative reconstructions. In Fig. 9(a), for example, the bedding poles do not fit to a vertical mean great circle (π-circle) which would be expected from a regular fold geometry. The normal to the π-circle plunges 23° towards N, which could indicate an overall tilt around an axis parallel to the π-circle subsequently to folding. The original publication did not consider the fold geometry or specify structural details. To examine the possibility of a fold plunge, the data set has been 'unplunged' stepwise (Figs 9b and c, and Table 2). During the tentative reconstruction, the A/n-value of the SCI fit rises and the k_m-value decreases, that is, the dispersion of the SCIs increases. Simultaneously, tilt-corrected remanence direction and SCI estimate drift away from each other. The actual data set has yet the least dispersion of intersections and the best coincidence of SCI estimate and tilt correction. The bedding geometry does, therefore, probably not represent a truly plunging fold and simple tilt correction is appropriate.

In the same way, it can be tested if deviating bedding strikes are the result of overall tilts. In the above example, the tentative reconstructions confirm that an overall tilt did not occur. The method can as well be applied to investigate the way of deformation, for example, whether apparently plunging fold structures are associated with regular tilting, tilting around inclined axes or due to an overall subsequent tilt.

Stewart (1995) and Pueyo *et al.* (2003) addressed this issue. Their basic idea is that tectonic tilt reconstruction with the wrong axes of rotation is likely to increase the dispersion of the corrected remanences. Trying different reconstructions with different axes and comparing the resulting remanence distributions shows which path is the likely one. The same procedure is possible with SCIs, which provide a further criterion to assess the likelyhood of reconstructions.

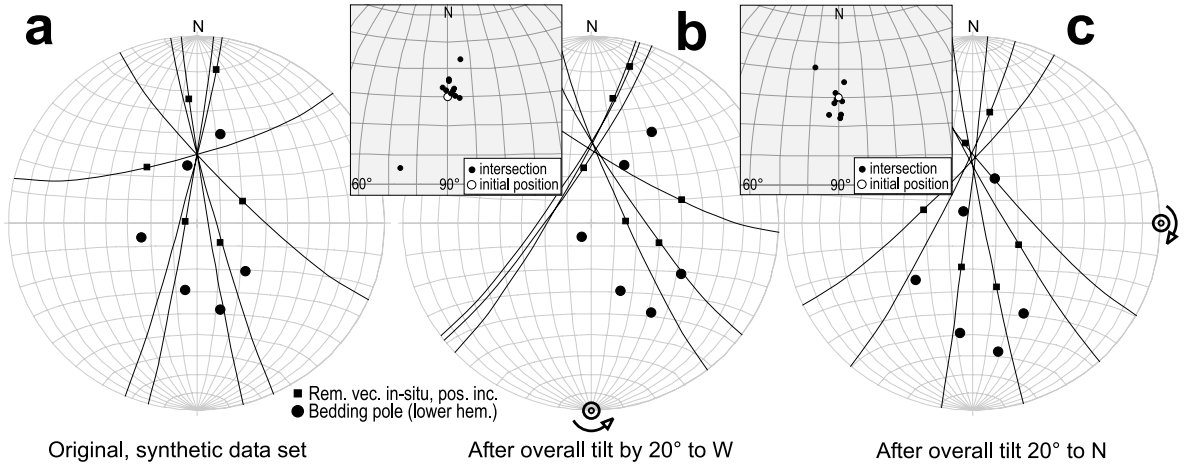

Figure 8. Theoretical effect of overall tilts on SCIs. Synthetic data. (a) Original array (zero remanence scatter) where all small circles intersect in a common point (15 coinciding intersections). (b) After overall tilt by 20° to W. (c) After overall tilt by 20° to N. Small figures on top left show intersections only, with initial position for comparison.

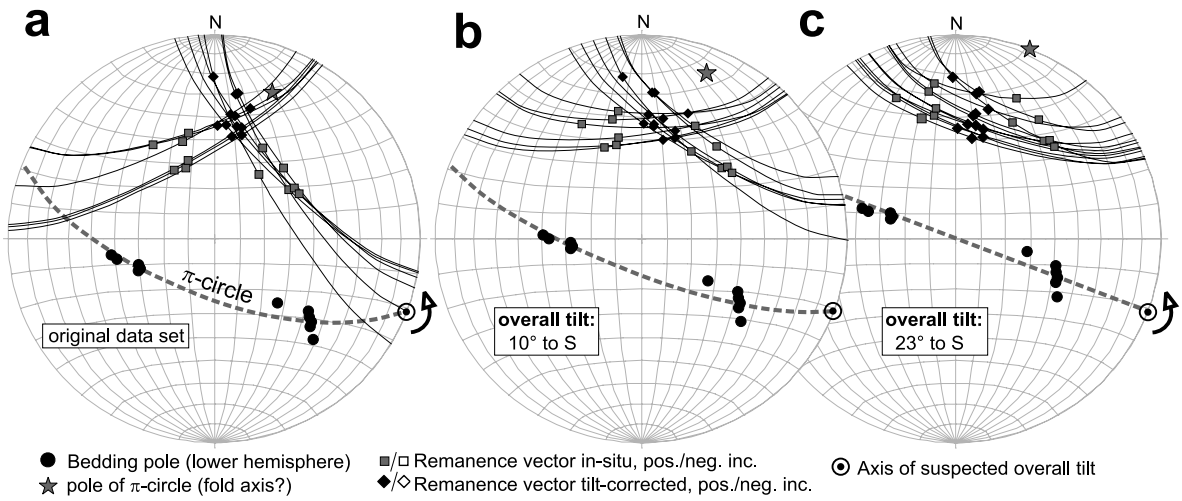

Figure 9. Tentative reconstruction by 'stepwise unplunging' to assess if an overall tilt due to fold plunge formation has affected the data set. (a) Data set '*Dadeli*' from Tamai *et al.* (2004). Pole of π-circle: azimuth: 21°, plunge: 23°; possible axis of overall tilt trends 111°. (b-c) Increasing dispersion of SCIs and tilt-corrected remanences (listed in Table 2) suggest that a true fold plunge is not given. Equal area projection.

Table 2. Progressive unplunging of the data of Fig. 9(a), with resulting SCI estimate and tilt-corrected Fisher mean. Axis for overall tilt: 111°. m_r: number of intersections in unit circle. k_m: modified concentration parameter according to Enkin *et al.* (2002) A/n: fit parameter of SCI, see appendix (A/n lower = intersections/small circles closer together). Angular diff.: angle (great circle segment) between palaeofield directions from SCI and tilt correction.

'Unplunging' by overall tilt	m_r	SCI estimate (D/I) with stat. parameters)	A/n	Tilt-corrected Fisher mean (D_s/I_s)	Angular diff.
unchanged		**12.6°/41.9° $k_m = 206$ $\alpha_{95} = 2.8°$**	**3.05°**	**8.5°/−38.5° $k = 81$ $\alpha_{95} = 4.8°$**	**4.6°**
5° to S (201°)	48	9.6°/43.9° $k_m = 158$ $\alpha_{95} = 3.2°$	3.46°	6.9°/38.6° $k = 53$ $\alpha_{95} = 6.0°$	5.7°
10° to S (201°)	46	12.9°/43.3° $k_m = 146$ $\alpha_{95} = 3.3°$	3.51°	7.6°/38.8° $k = 61$ $\alpha_{95} = 5.6°$	6.0°
15° to S (201°)	46	20.0°/42.8° $k_m = 133$ $\alpha_{95} = 3.5°$	3.57°	7.8°/38.8° $k = 69$ $\alpha_{95} = 5.3°$	10.1°
20° to S (201°)	35	34.2°/40.2° $k_m = 95$ $\alpha_{95} = 4.2°$	3.78°	8.1°/38.5° $k = 75$ $\alpha_{95} = 5.1°$	20.2°
23° to S (201°)	23	49.2°/32.4° $k_m = 100$ $\alpha_{95} = 4.1°$	4.55°	8.3°/38.7° $k = 76$ $\alpha_{95} = 5.0°$	33.6°

Fig. 10 gives the example of a data set from a strongly plunging fold (Hirt *et al.* 1992). With two other sites (AC27 and AC28) from this data set of the Asturian Arc, Stewart (1995) showed that the limbs of a plunging fold rotated around axes parallel to the fold hinge, and concluded that the fold plunge probably formed by an overall tilt perpendicular to the fold axis ('true plunging fold'). Here we took three other sites from this data set (because the two above sites only produce one intersection) where moreover azimuth and plunge of the fold axis were given (239°/62°), applied stepwise unplunging and observed the concentration of the tilt-corrected remanence directions (Stewart's method) and of the SCIs. Unplunging used the horizontal axis perpendicular to the measured fold axis (see Fig. 10). Both, tilt-corrected remanences and SCIs, move closer together and reach highest vicinity at 50° (remanences) and 55° (intersections) of unplunging (Fig. 10c), where also the fold axis comes close to horizontal. With complete unplunging by 62°, intersections and remanences remain quite similar. Thus, the two different methods coincide and indicate a similar fold plunge that corresponds reasonably well with the measured plunge of the fold hinge.

8 CONCLUSIONS

SCIs constitute an important feature in palaeomagnetism because they provide access to the palaeomagnetic field direction. For variably synfolding remanences, the SCI method is the only valid method. For pre-folding remanences, a further approach to the palaeofield direction is given which allows to cross-check tilt correction and fold tests. We revised more than 60 data sets from literature and found that in most cases the SCI method is applicable. In many of them, SCI is able to provide more information, either refining and/or enhancing reliability of interpretation. However, care is needed with SCI. It cannot be applied blindly and must never go without a close look to the local geological background, that is, the structure of bedding and the history of deformation. First of all, the remanence small circles have to intersect sufficiently, requiring sites with largely different bedding strikes. This has to be ensured by sampling. Second, relative rotations between sites or an overall tilt of whole or part of a data set are not allowed. Otherwise, the SCI estimate can be biased substantially or will just be unreliable. Also at shallow field inclinations, SCI estimates must be handled with care due to directional ambiguity of upper and lower hemisphere. To investigate if a data set is suitable for SCI and how reliable an SCI estimate is, intersections of remanence small circles provide an effective tool. Upon the application to more than 60 data sets, we found the following observations with respect to their occurrence and distribution:

(1) The overall number of actually realized versus theoretically possible intersections of a data set is a first, qualitative indicator of how good an SCI estimate will be. Where all or most intersections are found, SCI is most likely well constrained and also rooted broadly within a data set. With not more than half of the possible intersections or even less, SCI will unlikely provide a reliable result.

(2) The number of intersections on individual small circles indicates how important a small circle is for the SCI estimate. The more intersections a small circle has (the more others it crosses),

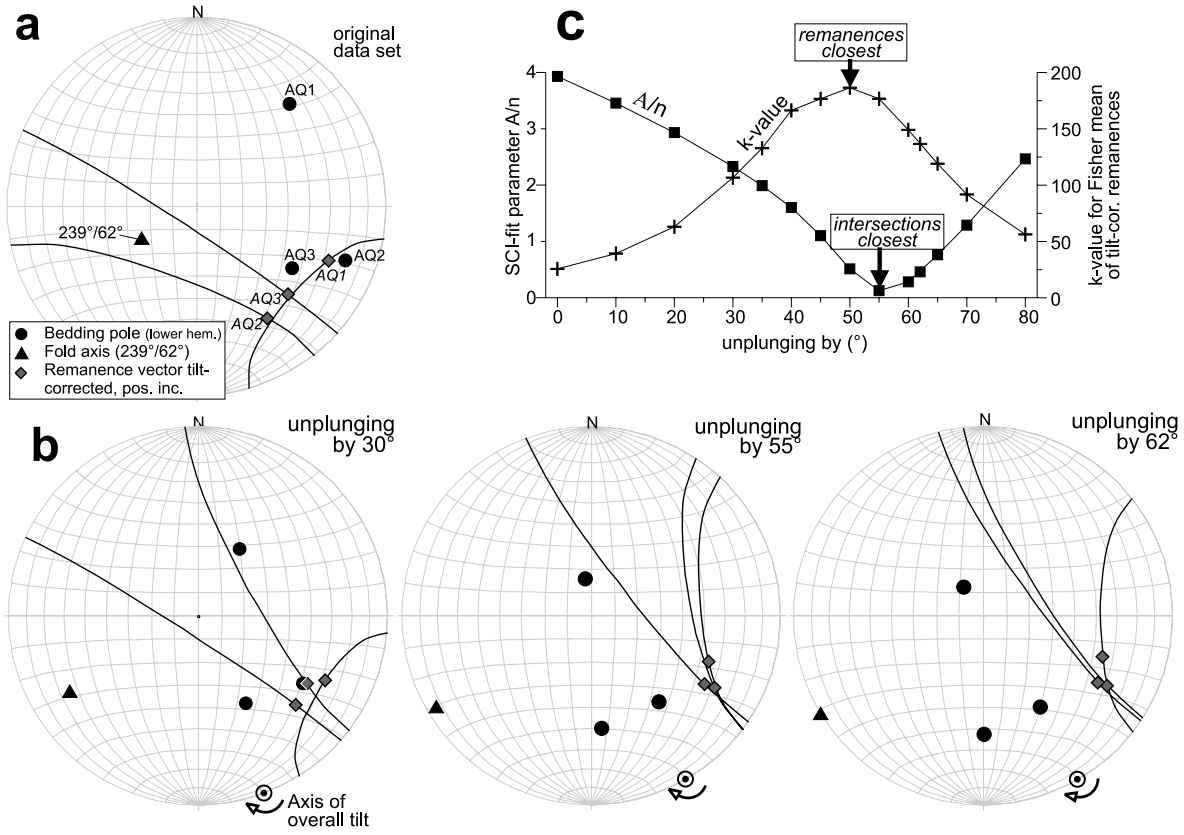

Figure 10. SCIs and remanences after tilt correction during stepwise unplunging of three sites from a plunging fold (data from Hirt *et al.* 1992). Values in Table 3. (a) Original data set. (b) Three exemplary steps of unplunging. Both, tilt-corrected remanences and SCIs, move closer together and reach highest vicinity at 50° (k-value) and 55° (A/n-value) of unplunging, where also the fold axis comes close to horizontal position. Remanence and intersection positions are very similar at complete unplunging by 62°. (c) A/n and k during stepwise unplunging. k: concentration parameter; A/n: fit parameter of SCI (see appendix).

the more influence it will have. By selectively removing such important small circles, it can be seen whether an SCI estimate is rooted broadly, or determined by only one or a few sites.

(3) The dispersion of SCIs is a qualitative indicator of irregular tectonic settings, that, together with other evidence like declination scatter, helps to identify relative rotations between the sites, oblique tilting or subsequent overall tilts. With well-grouping intersections and coinciding palaeofield directions from SCI and tilt correction, a data set did most likely not experience irregular displacements and is thus valid for SCI, tilt correction and Fisher statistics. On the other hand, with broadly scattered intersections, tectonic irregularities must come into consideration. Then neither SCI is valid nor Fisher statistics and fold tests. The data set must be investigated in more detail and with different methods. Tentative reconstructions using remanence vectors, SCIs and bedding poles can help to unravel the likely sequence of displacements.

We finally want to emphasize that the small circle methods shall not replace any conventional method in palaeomagnetism. SCI methods are geometrically alternative and, applied in addition, they allow for a more detailed and more reliable interpretation, giving rise also to new applications to tectonic problems. The small circle methods are moreover not restricted to palaeomagnetic data. They can analogously be used in the field of palaeostress analysis where recently tilt tests are becoming introduced (Yamaji *et al.* 2005) to see if fracture sets developed before, during or after folding.

ACKNOWLEDGMENTS

The manuscript benefited from discussions with W. Frisch, A. Patzelt and E. Waldhoer. The review of B. Henry of an earlier attempt helped to move the focus into the right direction. The final reviews and suggestions of B. Henry and S. Shipunov eventually solidified the concept and also indicated where to continue with further work. The project was financed by the German Research Foundation (DFG).

REFERENCES

Arriagada, C., Roperch, P. & Mpodozis, C., 2000. Clockwise block rotations along the eastern border of the Cordillera de Domeyko, Northern Chile (22°45′–23°30′S). *Tectonophysics,* **326,** 153–171.

Cairanne, C., Aubourg, C. & Pozzi, J.P., 2002. Syn-folding remagnetization and the significance of the small circle test: examples from the Vocontian trough (SE France), *Phys. Chem. Earth,* **27,** 1151–1159.

Channell, J.E.T., Brandner, R., Spieler, A. & Stoner, J.S., 1992a. Paleomagnetism and paleogeography of the Northern Calcareous Alps (Austria), *Tectonics,* **11**(4), 792–810.

Channell, J.E.T., Doglioni, C. & Stoner, J.S., 1992b. Jurassic and Cretaceous paleomagnetic data from the Southern Alps (Italy), *Tectonics,* **11**(4), 811–822.

Chen, Y., Cogné, J.-P. & Courtillot, V., 1992. New Cretaceous paleomagnetic poles from the Tarim Basin, Northwestern China, *Earth planet. Sci. Lett.,* **114,** 17–38.

Cogné, J.-P., Chen, Y., Courtillot, V., Rocher, F., Wang, G., Bai, M. & You, H., 1995. A paleomagnetic study of Mesozoic sediments from the Junggar and Turfan basins, northwestern China, *Earth planet. Sci. Lett.,* **133,** 353–366.

Delaunay, S., Smith, B. & Aubourg, C., 2002. Asymmetrical fold test in the case of overfolding: two examples from the Makran accretionary prism (Southern Iran), *Phys. Chem. Earth,* **27,** 1195–1203.

Enkin, R.J., 2003. The direction-correction tilt test: an all-purpose tilt/fold test for paleomagnetic studies, *Earth planet. Sci. Lett.,* **212,** 151–166.

Enkin, R.J. & Watson, G., 1996, Statistical analysis of palaeomagnetic inclination data, *Geophys. J. Int.,* **126,** 495–504.

Enkin, R.J., Osadetz, K.G., Baker, J. & Kisilevsky, D., 2000. Orogenic remagnetizations in the front ranges and inner foothills of the Southern Canadian Cordillera: chemical harbinger and thermal handmaiden of Cordilleran deformation, *GSA Bull.,* **112,** 929–942.

Enkin, R.J., Mahoney, J.B., Baker, J., Kiessling, M. & Haugerud, R.A., 2002. Syntectonic remagnetization in the southern Methow block: resolving large displacements in the southern Canadian Cordillera, *Tectonics,* **21**(4), 18-1–18-18.

Gough, D.I. & Opdike, N.D., 1963. The palaeomagnetism of the Lupata Alkaline Volcanics, *Geophys. J. R. astron. Soc.,* **7,** 457–468.

Haihong, C., Dobson, J., Heller, F. & Jie, H., 1995. Paleomagnetic evidence for clockwise rotation of the Simao region since the Cretaceous: A consequence of India-Asia collision, *Earth planet. Sci. Lett.,* **134,** 203–217.

Halim, N., Chen, Y. & Cogné, J.P., 2003. A first palaeomagnetic study of Jurassic formations from the Qaidam basin, Northeastern Tibet, China—tectonic implications, *Geophys. J. Int.,* **153,** 20–26.

Haubold, H., Scholger, R., Frisch, W., Summesberger, H. & Mauritsch, H.J., 1999. Reconstruction of the geodynamic evolution of the Northern Calcareous Alps by means of Paleomagnetism, *Phys. Chem. Earth (A),* **24**(8), 697–703.

Henry, B., Rouvier, H., Le Goff, M., Leach, D., Macquar, J.-C., Thibieroz, J. & Lewchuk, M.T., 2001. Palaeomagnetic dating of widespread remagnetization on the southeastern border of the French Massif Central and implications for fluid flow and Mississippi Valley-type mineralization, *Geophys. J. Int.,* **145,** 368–380.

Henry, B., Rouvier, H. & Le Goff, M., 2004. Using syntectonic remagnetizations for fold geometry and vertical axis rotation: the example of the Cévennes Border (France), *Geophys. J. Int.,* **157,** 1061–1070.

Hirt, A.M., Lowrie, W., Julivert, M. & Arboleya, M.L., 1992. Paleomagnetic results in support of a model for the origin of the Asturian arc, *Tectonophysics,* **213,** 321–339.

Huang, K., Opdyke, N.D., Peng, X. & Li, J., 1992. Paleomagnetic results from the Upper Permian of the eastern Qiantang Terrana of Tibet and their tectonic implications, *Earth planet. Sci. Lettr.,* **111,** 1–10.

Huang, B., Otofuji, Y., Yang, Z. & Zhu, R., 2000. New Silurian and Devonian palaeomagnetic results from the Hexi Corridor terrane, northwest China, and their tectonic implications, *Geophys. J. Int.,* **140,** 132–146.

Huang, B., Shi, R., Wang, Y. & Zhu, R., 2005. Palaeomagnetic investigation on Early-Middle Triassic sediments of the North China block: a new Early Triassic palaeopole and its tectonic interpretation, *Geophys. J. Int.,* **160,** 101–113.

Jordanova, N., Henry, B., Jordanova, D., Ivanov, Z., Dimov, D. & Bergerat, F., 2001. Paleomagnetism in nothwestern Bulgaria: geological implications of widespread remagnetization, *Tectonophysics,* **343,** 79–92.

Klootwijk, C.T. & Bingham, D.K., 1980. The extent of Greater India, III. Palaeomagnetic data from the Tibetan sedimentary series, Thakkhola Region, Nepal Himalaya, *Earth planet. Sci. Lett.,* **51,** 381–405.

Klootwijk, C.T., Conaghan, P.J., Nazirullah, R. & de Jong, K.A., 1994. Further palaeomagnetic data from Chitral (Eastern Hindukush): evidence for an early India-Asia contact, *Tectonophysics,* **237,** 1–25.

Kravchinsky, V.A., Cogné, J.-P., Harbert, W.P. & Kuzmin, M.I., 2002. Evolution of the Mongol–Okhotsk Ocean as constrained by new palaeomagnetic data from the Mongol–Okhotsk suture zone, Siberia, *Geophys. J. Int.,* **148,** 34–57.

Levashova, N.M., Degtyarev, K.E., Bazhenov, M.L., Collins, A.Q. & Van der Voo, R., 2003. Permian palaeomagnetism of East Kazakhstan and the amalgamation of Eurasia, *Geophys. J. Int.,* **152,** 677–687.

Lewchuk, M.T., Elmore, R.D. & Evans, M., 2002, Remagnetization signature of Paleozoic sedimentary rocks from the Patterson Creek Mountain anticline in West Virginia, *Phys. Chem. Earth,* **27,** 1141–1150.

Lewchuk, M.T., Evans, M. & Elmore, R.D., 2003. Synfolding remagnetization and deformation: results from Palaeozoic sedimentary rocks in West Virginia, *Geophys. J. Int.,* **152,** 266–279.

Lin Jinlu & Watts, D.R., 1988. Palaeomagnetic results from the Tibetan Plateau, *Phil. Trans. R. Soc. Lond.,* A, **327,** 239–262.

Liu, Y. & Morinaga, H., 1999. Cretaceous palaeomagnetic results from Hainan Island in south China supporting the extrusion model of Southeast Asia, *Tectonophysics,* **301,** 133–144.

MacDonald, W.D., 1980. Net tectonic rotation, apparent tectonic rotation, and the structural tilt correction in paleomagnetic studies, *J. geophys. Res.,* **85**(B7), 3659–3669.

Mac Niocaill, C., Smethurst, M.A. & Ryan, P.D., 1998. Oroclinal bending in the Caledonides of western Ireland: a Late-Palaeozoic feature controlled by a pre-existing structural grain, *Tectonophysics,* **299,** 31–47.

Mac Niocaill, C., 2000. A new Silurian palaeolatitude for eastern Avalonia and evidence for crustal rotations in the Avalonian margin of southwestern Ireland, *Geophys. J. Int.,* **141,** 661–671.

McClelland-Brown, E., 1983. Palaeomagnetic studies of fold development and propagation in the Pembrokeshire old red sandstone, *Tectonophysics,* **98,** 131–149.

McFadden, P.L., 1990. A new foldtest for palaeomagnetic studies, *Geophy. J. Int.,* **103,** 163–169.

Molina-Garza, R.S., Böhnel, H.N. & Hernández, T., 2003. Paleomagnetism of the Cretaceous Morelos and Mezcala Formations, southern Mexico, *Tectonophysics,* **361,** 301–317.

Niitsuma, S., Niitsuma, N. & Saito, K., 2003. Evolution of the Komiji Syncline in the North Fossa Magna, central Japan: paleomagnetic and K–Ar age insights, *The Island Arc,* **12,** 310–323.

Otofuji, Y., Funahara, S., Matsuo, J., Murata, F., Nishiyama, T., Zheng, X. & Yaskawa, K., 1989. Paleomagnetic study of western Tibet: deformation of a narrow zone along the Indus Zangboo suture between India and Asia, *Earth planet. Sci. Lettr.,* **92,** 307–316.

Patzelt, A., Li, H.M., Wang, J.D. & Appel, E., 1996. Palaeomagnetism of Cretaceous to Tertiary sediments from southern Tibet: evidence for the extent of the northern margin of India prior to the collision with Eurasia, *Tectonophysics,* **259**(4), 259–284.

Pueyo, E.L., 2000. Rotaciones paleomagnéticas en sistemas de pliegues y cabalgamientos. Tipos, causas, significado y aplicaciones (ejemplos de las Sierras Exteriores y de la Cuenca de Jaca, Pirineo Aragoneés), *PhD thesis,* University of Zaragoa, Spain, p. 296.

Pueyo, E.L., Parés, J.M., Millán, H. & Pocoví, A., 2003. Conical folds and apparent rotations in paleomagnetism (a case study in the Southern Pyrenees), *Tectonophysics,* **362,** 345–366.

Pueyo, E.L., Pocovi, A., Millan, H. & Sussman, A.J., 2004. Map-view models for correcting and calculating shortening estimates in rotated thrust fronts using paleomagnetic data, in *Orogenic Curvature: Integrating Paleomagnetic and Structural Analyses*, Vol. 383, pp. 1–15, eds Sussman, A.J. & Weil, A.B., Geological Society of America Special Paper.

Ramsay, J.G. & Huber, M.I., 1987, *The Techniques of Modern Structural Geology, Vol. 2: Folds and Fractures*, Academic Press, London, p. 700.

Schätz, M., Tait, J., Bachtadse, V., Heinisch, H. & Soffel, H., 2002. Palaeozoic geography of the Alpine realm, new palaeomagnetic data from the Northern Graywacke Zone, Eastern Alps, *Int. J. Earth Sci.,* **91,** 979–992.

Sharps, R., McWilliams, M., Li, Y., Cox, A., Zhang, Z., Zhai, Y., Gao, Z., Li, Y. & Li, Q., 1989. Lower Permian paleomagnetism of the Tarim block, northwestern China, *Earth planet. Sci. Lettr.,* **92,** 275–291.

Shipunov, S.V., 1997. Synfolding magnetization: detection, testing and geological applications, *Geophys. J. Int.,* **130,** 405–410.

Staiger, M., 2004. Palaeomagnetic and structural investigations in unbeknown areas of Central Tibet: a study on block rotations and crustal shortening, *PhD thesis,* p. 67, Univ. Tübingen, Germany.

Stewart, S.A., 1995. Palaeomagnetic analysis of plunging fold structures: Errors and a simple fold test, *Earth planet. Sci. Lett.,* **130,** 57–67.

Surmont, J., Sandulescu, M. & Bordea, S., 1990. Mise en évidence d'une réaimantation fini crétacée des séries mésozoiques de l'unité de Bihor

(Monts Apuseni, Roumanie) et de sa rotation horaire ultérieure, *C. R. Acad. Sci. Paris,* **310,** Série II, 213–219.

Tamai, N., Liu, Y., Zong Lu, L., Yokoyama, M., Halim, N., Zaman, H. & Otofuji, Y., 2004. Palaeomagnetic evidence for southward displacement of the Chuan Dian fragment of the Yangtze Block, *Geophys. J. Int.,* **158,** 297–309.

Thomas, J.C., Chauvin, A., Gapais, D., Bazhenov, M.L., Perroud, H., Cobbold, P.R. & Burtman, V.S., 1994. Paleomagnetic evidence for Cenozoic block rotations in the Tadjik depression (Central Asia), *J. geophys. Res.,* **99**(B8), 15 141–15 160.

Thomas, J.C., Claudel, M.E., Collombet, M., Tricart, P., Chauvin, A. & Dumont, T., 1999. First paleomagnetic data from the sedimentary cover of the French Penninic Alps: evidence for Tertiary counterclockwise rotations in the Western Alps, *Earth planet. Sci. Lettr.,* **171,** 561–574.

Uno, K., 1999. Early Triassic palaeomagnetic results from the Ryeongnam Block, Korean Peninsula: the eastern extension of the North China Block, *Geophys. J. Int.,* **139,** 841–851.

Uno, K., Chang, T.W. & Furukawa, K., 2004. Tectonic elements with South China affinity in the Korean Peninsula: new Early Jurassic palaeomagnetic data, *Geophys. J. Int.,* **158,** 446–456.

Waldhör, M., Appel, E., Frisch, W. & Patzelt, A., 2001. Palaeomagnetic investigation in the Pamirs and its tectonic implications, *J. Asian Earth Sci.,* **19,** 429–451.

Yamaji, A., Satoshi, T. & Otsubo, M., 2005. Bedding tilt test for paleostress analysis, *J. Struct. Geology,* **27,** 161–170.

Zwing, A., Bachtadse, V. & Soffel, H.C., 2002. Late Carboniferous remagnetisation of Palaeozoic rocks in the NE Rhenish Massif, Germany, *Phys. Chem. Earth,* **27,** 1179–1188.

APPENDIX A: MODIFICATION OF THE METHOD OF SHIPUNOV (1997)

Henry *et al.* (2004) noted that an estimate according to the method of Shipunov (1997) could be biassed, because it minimises distances in the x-y plane of the unit sphere and not angles (Fig. A1a). Shipunov's method finds the point $[x,y]$ that is closest to n small circles by minimising the sum of squares S of the distances s_n in Cartesian coordinates:

$$S = \sum s_n^2 = \sum (a_n X + b_n Y + d_n)^2 \rightarrow \min$$

$$\times \text{ (equations A2 and A3 from Shipunov 1997)}$$

with $a_n = \sin \tau_n$, $b_n = \cos \tau_n$ (τ_n trend of tilt axis) and $d_n = \cos(\tau_n - D_n) \cdot \cos I_n$ (d_n distance between small circle and origin; D_n / I_n declination and inclination of remanence vector on the small circle). The field estimate is obtained by vertical orthographic back-projection to the sphere's surface. However, this field direction is not located at minimum angles (great circle segments) to each remanence small circle. Alternatively, instead of minimising the distances s_n, the angles (great circle segments) between remanence small circles and point $[x,y]$ can be minimised. The angle α_n is given by (see Fig. A1b):

$$\alpha_n = \arcsin(d_n) - \arcsin(d_n - s_n) = \arcsin(d_n) - \arcsin(a_n x + b_n y) \quad \text{(A1)}$$

The direction located at optimum angles is iteratively resolved by minimising the sum A of the amount of the angles α_n:

$$A = \sum |\alpha_n| \rightarrow \min \quad \text{(A2)}$$

The obtained $[x,y]$-point is back-projected to the sphere's surface to give the estimate of the field direction. Statistical parameters k_m and α_{95} according to Enkin *et al.* (2002) are derived by averaging the vector directions closest to the field estimate on each small circle. To compare different SCI-estimates, *A/n* should be used. In addition to iterative minimisation, *A/n* can be calculated for a densely spaced grid of x-y-coordinates within the unit projection circle. Then a contour plot will illustrate perspicuously to where and how sharply an SCI-estimate converges. Spreadsheets for calculation of SCI-estimates and small circle intersections can be downloaded from:

http://www.uni-tuebingen.de/geo/gpi/ag-appel/projekte/palaeomag/smallcircles/

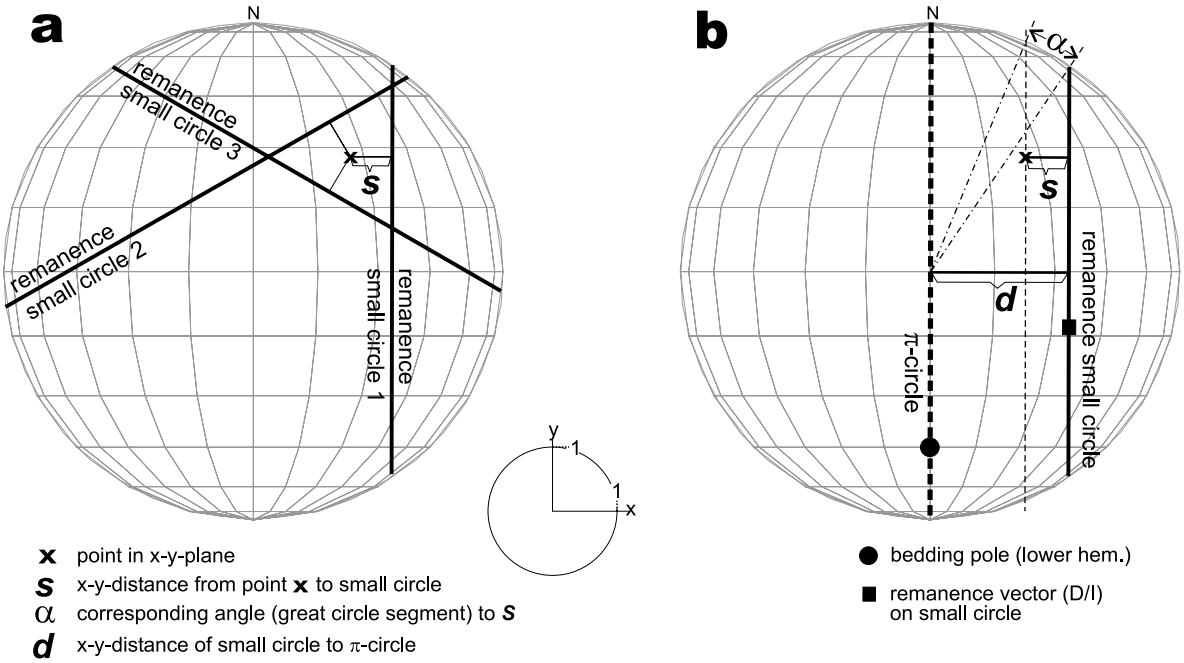

Figure A1. (a) Determination of the best-fit point **x** with respect to $x--y$-distances ***s*** (Cartesian coordinates) for three remanence small circles according to Shipunov (1997). $x--y$ distance as fraction of the radius $r = 1$. (b) Determining the angle $\boldsymbol{\alpha}$ between remanence small circle and $x--y$-estimate. Orthographic projections.